Taylor & Francis
Taylor & Francis Group

Molecular mechanics simulations of graphene using finite elements

T.C. Theodosiou* and D.A. Saravanos

Department of Mechanical & Aeronautics Engineering, University of Patras, Rion-Patras, Greece

This paper demonstrates a modelling approach for graphene and related nanostructures by embedding molecular mechanics equations into finite element codes. Atomistic interactions are modelled using specialty finite elements, based on analytical expressions of molecular mechanics equations. The major advantages of the proposed approach can be summarised as: (i) direct integration into well-established software; (ii) more realistic representation than other similar approaches; and (iii) user-friendly way to create an atomistic structure. Examples of incorporating the developed finite elements into Abaqus are also demonstrated. The introduced approach does not claim to replace other well-established molecular mechanics/dynamics software, but to provide a more intuitive structural modelling approach for graphene.

Keywords: graphene; molecular mechanics; specialty finite elements

Introduction

Graphite monolayer, or graphene, is one of the most theoretically analysed materials in the literature as the basis for the analysis of other nanocarbons like carbon nanotubes, fullerenes, etc. The recent discovery of its stable crystalline form (Gaim & Novoselov, 2007) has triggered a whole new research effort targeting graphene itself. Numerous applications have already been proposed; the already proven mechanical and electrical properties (Geim, 2009) have boosted the efforts towards the development of nano-electro-mechanical devices (Poetscke, Rocha, Foa Torres, Roche, & Cuniberti, 2010; Shi et al., 2012), while novel applications have been envisioned regarding energy production, storage and conversion (Brownson, Kampouris, & Banks, 2011; Sun, Wu, & Shi, 2011).

The traditional modelling tools including molecular dynamics, Density Functional Theory (DFT) calculations, tight-binding, *ab initio* methods, etc. have been successfully implemented by various researchers and the properties of graphene have been predicted. However, their use becomes rather impractical for studying a material in microscale. In addition, the assumptions made during a molecular simulation, like periodicity and structural integrity, may not apply in a real case making predictions invalid and leading to faulty material modelling. Another issue is that microscale material modellers are not always familiar with the details of nanoscale simulations and their range of validity, leading to scale mismatches and incompatibilities. Most of the available molecular mechanics software packages are designed to treat atomistic structures as a whole and provide no capability to apply concentrated loads on indi-

---

*Corresponding author. Email: dozius@mech.upatras.gr

vidual atoms or regions. However, sometimes it is necessary to perform localised structural investigations.

In order to alleviate such issues, various approaches have been proposed. Homogenising techniques (Caillerie, Mourad, & Raoult, 2006; Le Dret & Raoult, 2011) have become popular; this approach replaces the discrete graphitic lattice with an effective medium. Graphene is thus replaced by an equivalent continuum (Avila, Eduardo, & Neto, 2011). Another efficient approach is the use of finite element methods by taking advantage of similarities in molecular mechanics. A specialty molecular finite element based on the repetitive hexagonal pattern of the graphitic lattice has been reported (Theodosiou & Saravanos, 2007). Another common method is to replace stretching, bending and torsion energy terms with an effective beam element whose nodes represent carbon atoms (Parvaneh, Shariati, Torabi, & Sabeti, 2012; Tserpes, 2012). Although these approaches are relatively easy to implement, various questions rise concerning their degree of realistic representation of the atomic interactions in the equilibrium equation, especially for the modelling of bending, torsion and non-bonded energy terms. For instance, for a pair of atoms represented with a two-node beam element, bending stiffness is expected. However, in nature, this type of interaction is only activated by the presence of a third atom.

The approach presented in the following sections is based entirely on molecular mechanics equations and has the following advantages: (i) interactions are calculated analytically. The interatomic potential is calculated using a well-established formulation, whose derivation directly provides nodal forces without the need of numerical interpolation. (ii) The molecular mechanics formulation provides analytical expressions for the imbalance vector and stiffness matrix of the structure, leading to faster solution convergence. (iii) Atomic interactions are modelled in a realistic way, i.e. as atomic forces/moments and not as an effective continuum. Moreover, this approach allows for incorporation into well-established commercial software which provides additional benefits like, (i) use of optimised solvers and computational techniques, (ii) direct connection to other finite element (FE) models, (iii) assembly of nano/ micro-structures, etc.

Modelling approach

Molecular mechanics formulation

For the needs of the present work, the total energy of the system V due to the atomic interactions has been expressed as the sum of numerous energy terms:

$$V = V_{str} + V_{ang} + V_{dih} + V_{vdw} \tag{1}$$

following a Morse-type formulation in the respective energy terms included in Equation (1); subscripts "str", "ang", "dih" and "vdw" express bond stretching, angle bending, dihedral angles and non-bonded interactions, respectively. Alternative energy formulations may be successfully employed as well (Brenner, 1990). However, the use of Morse-type potential may easier lead to conclusions about the effects of each interaction mechanism. Analytical expressions for each term will be reported within the context of element descriptions, while the parameter set used is enlisted in Table 1 (Natsuki & Endo, 2004; Sakhaee-Pour, Ahmadian, & Naghdabadi, 2008). The equilibrium state under any loading can be identified by minimising Equation (1).

The equilibrium equations can be obtained in variational form from the minimisation of the total energy (Π):

Table 1. Parameter set used for the calculations required by Equation (1).

Parameter	Value
D_e	1.807 eV
β	38.43 nm
r_0	0.142 nm
k_θ	5.617 eV rad^{-2}
k_s	0.754 rad^{-4}
θ_0	$2\pi/3$
k_d	1.735 eV rad^{-2}
φ_0	0
σ	0.34 nm
ε	2.41265e–3 eV

$$\min(\Pi) = \min(V - \mathbf{F} \cdot \mathbf{u}), \tag{2}$$

where V is the total energy as calculated by Equation (1), $\mathbf{F}$ is the vector of the external forces and $\mathbf{u}$ are the atomic displacements, using extended vector notation.

Using a Taylor expansion series, the total energy can be recast:

$$\Pi = \Pi_0 + \frac{\partial \Pi}{\partial \mathbf{u}} \cdot d\mathbf{u} + \frac{1}{2} \cdot d\mathbf{u}^T \cdot \frac{\partial^2 \Pi}{\partial \mathbf{u}} \cdot d\mathbf{u} + \cdots \tag{3}$$

The following quantities can be then introduced:

$$\boldsymbol{\psi} = \frac{\partial \Pi}{\partial \mathbf{u}}, \tag{4}$$

$$[\bar{\mathbf{K}}] = \frac{1}{2} \cdot \frac{\partial^2 \Pi}{\partial \mathbf{u}^2}. \tag{5}$$

Therefore, Equation (3) becomes:

$$\Pi = \Pi_0 + \boldsymbol{\psi} \cdot d\mathbf{u} + d\mathbf{u}^T \cdot [\bar{\mathbf{K}}] \cdot d\mathbf{u}. \tag{6}$$

From Equations (2) and (4), it is clear that:

$$\boldsymbol{\psi} = \frac{\partial \Pi}{\partial \mathbf{u}} = \frac{\partial}{\partial \mathbf{u}}(V - \mathbf{F} \cdot \mathbf{u}) = \frac{\partial V}{\partial \mathbf{u}} - \mathbf{F}. \tag{7}$$

Vector $\boldsymbol{\psi}$ expresses the equilibrium between internal and external forces and it is termed Imbalance Vector, while $[\bar{\mathbf{K}}]$ in Equation (5) is actually a linearised (tangential) stiffness matrix.

According to the Principle of Virtual Works, the work produced by a virtual displacement $d\mathbf{u}$ will be:

$$\delta\Pi = d\mathbf{u} \cdot \boldsymbol{\psi} + d\mathbf{u} \cdot ([\bar{\mathbf{K}}] \cdot d\mathbf{u}), \tag{8}$$

as derived from Equation (6).

There are numerous methods to predict the atomic positions in the equilibrium state. The simplest one is perhaps the Newton–Raphson method or one of its modified variants (Suli & Mayers, 2003; Ypma, 1995). First, the atomic positions are roughly estimated. A better estimate is obtained if a corrective term $d\mathbf{u}$ is added to the vector of atomic positions. This term is calculated in Equation (8) by setting $\delta\Pi = \Pi - \Pi_0 = 0$:

$$[\bar{\mathbf{K}}] \cdot d\mathbf{u} = -\psi. \tag{9}$$

Equation (9) can be used repeatedly until the optimal equilibrium state is obtained.

Finite element approach

Instead of performing energy minimisation on the whole system, the graphitic lattice can be diminished to an assembly of special finite elements, each one describing an individual energy term in Equation (1). Then, the elemental stiffness matrices can be used to assemble the global ones, which can be used in Equation (9) for the calculation of the equilibrium state.

The following part describes the details of the developed finite elements. Each element is uniquely identified in this work using the notation "Un", where n is a unique integer, e.g. U1, U2, etc. Although this is a custom notation, n has been properly selected to reflect the number of nodes composing each element. It is assumed that each atom coincides with an elemental node, so that the solution of the finite element system automatically provides the respective atomic configuration. Another assumption is that each node has three degrees of freedom corresponding to motion along the axes of the global Cartesian system (x, y, z). This implies that self-rotation of atoms is not accounted for. The latter assumption has no impact in calculations; as shown later, all needed quantities are expressed in terms of interatomic distances and nodal Cartesian coordinates, therefore, rotational degrees of freedom have been ignored, in order to limit the required amount of computational resources.

In order to express all derivatives in terms of Cartesian coordinates, the chain rule has been successively applied. The extent of the analytical expressions is prohibitive considering paper size limitations, thus, only a couple of force and stiffness terms are presented for each element in order to demonstrate the length and complexity of the derived expressions. However, all terms may be provided in their analytical form upon request.

Bond stretching interactions

Atomic bonds are pair wise interactions including atoms connected with a covalent bond. A special two-node element is necessary, termed thereafter as U2. Each atom is represented by an elemental node (Figure 1). The interaction between the two atoms is described by:
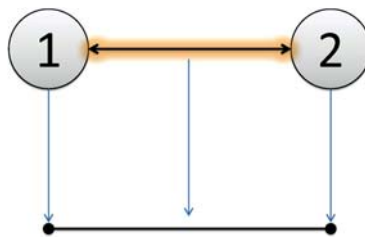
Figure 1.   Representation of the bond stretching interaction with a U2 element.

$$V_{\text{str}}(r) = D_e \cdot \left\{ \left[1 - e^{-\beta(r-r_0)} \right]^2 - 1 \right\}. \tag{10}$$

The element length is actually the interatomic distance required in the previous equation. Assuming nodes 1 and 2 are located at points $\mathbf{p_1}(x_1, y_1, z_1)$ and $\mathbf{p_2}(x_2, y_2, z_2)$, respectively, the interatomic distance is clearly:

$$r = \sqrt{(x_2 - x_1)^2 + (y_2 - y_1)^2 + (z_2 - z_1)^2}, \tag{11}$$

thus, the force on node 1 along x direction is:

$$(f_1^{\text{str}})_x = -\frac{\partial V_{\text{str}}}{\partial x_1} = -\frac{\partial V_{\text{str}}}{\partial r} \cdot \frac{\partial r}{\partial x_1} = 2 \cdot D_e \cdot b \cdot e^{-b(r-r_0)} \cdot \left[e^{-b(r-r_0)} - 1 \right] \cdot \frac{(x_1 - x_2)}{r}, \tag{12}$$

while the first term of its stiffness matrix is:

$$\begin{aligned}
k_{11} &= \frac{\partial^2 V_{\text{str}}}{\partial x_1^2} = \frac{\partial}{\partial x_1} \left[\frac{\partial V_{\text{str}}}{\partial x_1} \right] \\
&= \frac{2 \cdot D_e \cdot b^2 \cdot e^{2b(r_0-r)} \cdot (x_1 - x_2)^2}{r^2} - \frac{2 \cdot D_e \cdot b \cdot e^{b(r_0-r)} \cdot \left[e^{b(r_0-r)} - 1 \right]}{r} \\
&\quad + \frac{2 \cdot D_e \cdot b^2 \cdot e^{b(r_0-r)} \cdot \left[e^{b(r_0-r)} - 1 \right] \cdot (x_1 - x_2)^2}{r^2} \\
&\quad + \frac{2 \cdot D_e \cdot b \cdot e^{b(r_0-r)} \cdot \left[e^{b(r_0-r)} - 1 \right] \cdot (x_1 - x_2)^2}{r^3}.
\end{aligned} \tag{13}$$

In the same sense, all force and stiffness components can be analytically calculated, leading to a 6×1 force vector and a 6×6 stiffness matrix.

Angle bending interactions

Angle bending is actually the interaction of two bonded pairs sharing a common atom (Figure 2). A three-node element is therefore necessary, termed thereafter as U3. The energy term involved can be expressed as:

$$V_{\text{ang}}(\theta) = \frac{1}{2} k_\theta (\theta - \theta_0)^2 \left[1 + k_s (\theta - \theta_0)^4 \right], \tag{14}$$
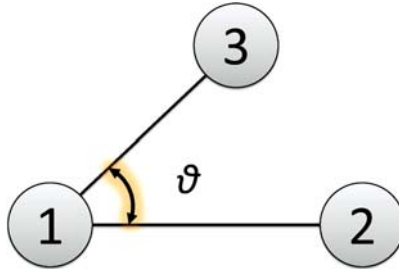
Figure 2. Definition of the angle included in angle bending calculations.

where θ is the angle formed by the two bonds. Assuming nodes 1, 2 and 3 are located at points $\mathbf{p_1}(x_1, y_1, z_1)$, $\mathbf{p_2}(x_2, y_2, z_2)$ and $\mathbf{p_3}(x_3, y_3, z_3)$, respectively, the angle θ can be expressed in terms of the Cartesian coordinates as:

$$\theta = \cos^{-1}\left[\frac{(\mathbf{p_2} - \mathbf{p_1}) \cdot (\mathbf{p_3} - \mathbf{p_1})}{|\mathbf{p_2} - \mathbf{p_1}| \cdot |\mathbf{p_3} - \mathbf{p_1}|}\right], \tag{15}$$

while the atomic distances will be:

$$r_{21} = r_{12} = |\mathbf{p_2} - \mathbf{p_1}|, \tag{16}$$

$$r_{31} = r_{13} = |\mathbf{p_3} - \mathbf{p_1}|. \tag{17}$$

The first force term for this element is provided by:

$$(f_1^{\text{ang}})_x = -\frac{\partial V_{\text{ang}}}{\partial x_1} = 2 \cdot \frac{k_s \cdot k_\theta \cdot A_1 \cdot A_2^5}{A_3} + \frac{k_\theta \cdot A_2 \cdot (k_s \cdot A_2^4 + 1) \cdot A_1}{A_3}, \tag{18}$$

where

$$A_1 = \frac{x_2 - 2x_1 + x_3}{r_{12} \cdot r_{13}} + \frac{2 \cdot (x_1 - x_2) \cdot A_4}{2 \cdot r_{12}^3 \cdot r_{13}} + \frac{2 \cdot (x_1 - x_3) \cdot A_4}{2 \cdot r_{12} \cdot r_{13}^3}, \tag{19}$$

$$A_2 = \theta_0 - \cos^{-1}\left(\frac{A_4}{r_{12} \cdot r_{13}}\right), \tag{20}$$

$$A_3 = \sqrt{1 - \frac{A_4^2}{r_{12} \cdot r_{13}}}, \tag{21}$$

$$A_4 = (x_1 - x_2)(x_1 - x_3) + (y_1 - y_2)(y_1 - y_3) + (z_1 - z_2)(z_1 - z_3), \tag{22}$$

while the first stiffness term:

$$\begin{aligned}
k_{11} &= \frac{\partial^2 V_{\text{ang}}}{\partial x_1^2} = \frac{\partial}{\partial x_1}\left[\frac{\partial V_{\text{ang}}}{\partial x_1}\right] \\
&= \frac{2 \cdot k_s \cdot k_\theta \cdot B_{12}^5 \cdot B_1}{\sqrt{B_6}} - \frac{k_\theta \cdot B_4 \cdot B_2^2}{B_5} + \frac{k_\theta \cdot B_{12} \cdot B_4 \cdot B_1}{\sqrt{B_6}} - \frac{14 \cdot k_s \cdot k_\theta \cdot B_{12}^4 \cdot B_2^2}{B_5} \\
&\quad + \frac{k_s \cdot k_\theta \cdot B_{12}^5 \cdot B_3 \cdot B_2}{\sqrt{B_6^3}} + \frac{k_\theta \cdot B_{12} \cdot B_4 \cdot B_3 \cdot B_2}{2\sqrt{B_6^3}},
\end{aligned} \tag{23}$$

where

$$B_1 = \frac{2}{r_{12} \cdot r_{13}} - \frac{A_4}{B_8} - \frac{A_4}{B_7} + \frac{3 \cdot B_{10}^2 \cdot A_4}{4 \cdot r_{12}^5 \cdot r_{13}} + \frac{3 \cdot B_9^2 \cdot A_4}{4 \cdot r_{12} \cdot r_{13}^5} + \frac{B_{10} \cdot B_{11}}{B_7} + \frac{B_9 \cdot B_{11}}{B_8} + \frac{B_{10} \cdot B_9 \cdot A_4}{2 \cdot r_{12}^3 \cdot r_{13}^3}, \tag{24}$$

$$B_2 = \frac{B_{11}}{r_{12} \cdot r_{13}} + \frac{B_{10} \cdot A_4}{2 \cdot r_{12}^3 \cdot r_{13}} + \frac{B_9 \cdot A_4}{2 \cdot r_{12} \cdot r_{13}^3}, \tag{25}$$

$$B_3 = \frac{2 \cdot B_{11} \cdot A_4}{r_{12}^2 \cdot r_{13}^2} + \frac{B_{10} \cdot A_4^2}{r_{12}^4 \cdot r_{13}^2} + \frac{B_9 \cdot A_4^2}{r_{12}^2 \cdot r_{13}^4}, \tag{26}$$

$$B_4 = k_s \cdot A_2^4 + 1, \tag{27}$$

$$B_5 = \frac{A_4^2}{r_{12}^2 \cdot r_{r13}^2} - 1, \tag{28}$$

$$B_6 = 1 - \frac{A_4^2}{r_{12}^2 \cdot r_{13}^2}, \tag{29}$$

$$B_7 = r_{12}^3 \cdot r_{13}, \tag{30}$$

$$B_8 = r_{12} \cdot r_{13}^3, \tag{31}$$

$$B_{10} = 2(x_1 - x_2), \tag{32}$$

$$B_{11} = x_2 - 2x_1 + x_3. \tag{33}$$

In the same way, all force and stiffness components can be analytically calculated leading to a 9×1 force vector and a 9×9 stiffness matrix.

Dihedral angle interactions

Interactions become more complicated when dihedral angles are included. Each angle formed by three atoms (as in angle bending interactions) defines a plane. Two angles sharing a common side (Figure 3) define two planes intersecting along the direction of the common side. A four-node element is therefore necessary, termed thereafter as U4. The angle φ formed by the two intersecting planes defines the respective energy term:

$$V_{\text{dih}}(\varphi) = \frac{1}{2}k_d(\varphi - \varphi_0)^2. \tag{34}$$
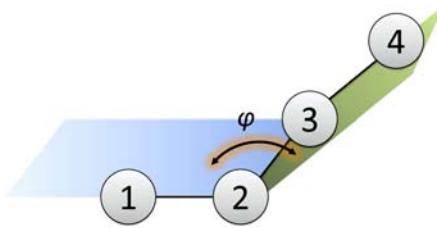
Figure 3.   Definition of a dihedral angle.

Assuming that the relative positions of the atoms are

$$\mathbf{R} = \mathbf{p_2} - \mathbf{p_1} \quad \mathbf{S} = \mathbf{p_3} - \mathbf{p_2} \quad \mathbf{Q} = \mathbf{p_4} - \mathbf{p_3}, \tag{35}$$

where $\mathbf{p_i}(x_i, y_i, z_i)$ is the position of the i-th atom, the dihedral angle is defined as:

$$\varphi = \tan^{-1}\left[\frac{S \cdot \mathbf{R} \cdot (\mathbf{S} \times \mathbf{Q})}{(\mathbf{R} \times \mathbf{S}) \cdot (\mathbf{S} \times \mathbf{Q})}\right], \tag{36}$$

where the S denotes the magnitude of vector $\mathbf{S}$ and the respective interatomic distances between atoms i and j are:

$$r_{ij} = r_{ji} = |\mathbf{p}_i - \mathbf{p}_j|, \tag{37}$$

Differentiation with respect to atomic coordinates leads to a 12×1 force vector and a 12×12 stiffness matrix. The first force term is expressed as:

$$(f_1^{\text{dih}})_x = -\frac{\partial V_{\text{dih}}}{\partial x_1} = -k_d \cdot \frac{\frac{C_1 \cdot C_4}{C_2} - \frac{[(y_2 - y_3) \cdot C_6 + (z_2 - z_3) \cdot C_5] \cdot C_3 \cdot C_1}{C_2^2} \cdot \left[\varphi_0 + \tan^{-1}\left(\frac{C_3 \cdot C_1}{C_2}\right)\right]}{\frac{C_3^2 \cdot C_1^2}{C_2^2} + 1}, \tag{38}$$

where

$$C_1 = r_{23}, \tag{39}$$

$$C_2 = \frac{4}{\left\{\begin{array}{c} [(x_1 - x_2)(y_2 - y_3) - (x_2 - x_3)(y_1 - y_2)] \cdot C_6 + \\ +[(x_1 - x_2)(z_2 - z_3) - (x_2 - x_3)(z_1 - z_2)] \cdot C_5 + \\ +[(y_1 - y_2)(z_2 - z_3) - (y_2 - y_3)(z_1 - z_2)] \cdot C_6 \end{array}\right\}}, \tag{40}$$

$$C_3 = (z_1 - z_2) \cdot C_6 - (y_1 - y_2) \cdot C_5 + (x_1 - x_2) \cdot C_4, \tag{41}$$

$$C_4 = (y_2 - y_3)(z_3 - z_4) - (y_3 - y_4)(z_2 - z_3), \tag{42}$$

$$C_5 = (x_2 - x_3)(z_3 - z_4) - (x_3 - x_4)(z_2 - z_3), \tag{43}$$

$$C_6 = (x_2 - x_3)(y_3 - y_4) - (x_3 - x_4)(y_2 - y_3), \tag{44}$$

and the first stiffness term:

$$\begin{aligned} k_{11} &= \frac{\partial^2 V_{\text{dih}}}{\partial x_1^2} = \frac{\partial}{\partial x_1}\left[\frac{\partial V_{\text{dih}}}{\partial x_1}\right] \\ &= \frac{k_d \cdot D_1^2}{D_2^2} + \frac{k_d \cdot \left[\frac{2 \cdot D_4^2 \cdot D_6 \cdot \sqrt{D_7}}{D_5^3} - \frac{2 \cdot D_4 \cdot D_8 \cdot \sqrt{D_7}}{D_5^2}\right]}{D_2} - \frac{k_d \cdot \left[\frac{2 \cdot D_8 \cdot D_6 \cdot D_7}{D_5^2} - \frac{2 \cdot D_4 \cdot D_6^2 \cdot D_7}{D_5^3}\right] \cdot D_1 \cdot D_3}{D_2^2}, \end{aligned} \tag{45}$$

where

$$D_1 = \frac{D_8 \cdot \sqrt{D_7}}{D_5} - \frac{D_4 \cdot D_6 \cdot \sqrt{D_7}}{D_5^2}, \tag{46}$$

$$D_2 = \frac{D_6^2 \cdot D_7}{2} + 1, \tag{47}$$

$$D_3 = \varphi_0 + \tan^{-1}\left(\frac{D_6 \cdot \sqrt{D_7}}{D_5}\right), \tag{48}$$

$$D_4 = (y_2 - y_3) \cdot D_{10} + (z_2 - z_3) \cdot D_9, \tag{49}$$

$$\begin{aligned} D_5 = {}& [(x_1 - x_2)(y_2 - y_3) - (x_2 - x_3)(y_1 - y_2)] \cdot D_{10} + \\ &+ [(x_1 - x_2)(z_2 - z_3) - (x_2 - x_3)(z_1 - z_2)] \cdot D_9 + \\ &+ [(y_1 - y_2)(z_2 - z_3) - (y_2 - y_3)(z_1 - z_2)] \cdot D_8, \end{aligned} \tag{50}$$

$$D_6 = (z_1 - z_2) \cdot D_{10} - (y_1 - y_2) \cdot D_9 + (x_1 - x_2) \cdot D_8, \tag{51}$$

$$D_7 = r_{23}^2, \tag{52}$$

$$D_8 = (y_2 - y_3)(z_3 - z_4) - (y_3 - y_4)(z_2 - z_3), \tag{53}$$

$$D_9 = (x_2 - x_3)(z_3 - z_4) - (x_3 - x_4)(z_2 - z_3), \tag{54}$$

$$D_{10} = (x_2 - x_3)(y_3 - y_4) - (x_3 - x_4)(y_2 - y_3), \tag{55}$$

Non-bonded interactions

Non-bonded interactions include interactions among atoms not connected by a covalent bond. For the needs of the present approach, only the van der Waals type of interaction is considered as described by the Lennard-Jones pair potential (Jones, 1924):

$$V_{\text{vdw}}(r) = 4\varepsilon \cdot \left[\left(\frac{\sigma}{r}\right)^{12} - \left(\frac{\sigma}{r}\right)^6 \right]. \tag{56}$$

The parameter values for Equation (56) are enlisted in Table 1, as well. Although a simple nonlinear truss element like U2 based on Equation (56) would be sufficient, a non-bonded interactions finite element has been developed targeting computational efficiency. The number of nodes composing this element can vary depending on the required accuracy. Since the number of nodes is not strictly defined, this element will be referenced as U99. As stated before, the obvious formulation of the U99 element would be the same as U2 using Equation (56) instead of Equation (10). For a system of N atoms, the number of U99 elements to be defined would be in the order of:

$$\binom{N}{2} = \frac{N \cdot (N-1)}{2}, \tag{57}$$

which is both impractical and computationally demanding for large systems. In order to increase the computational efficiency of the finite element, various assumptions have to be made: (i) each atom interacts only with atoms within a finite area. This limits the amount of calculations that need to be performed and is in agreement with other successful models (Brenner, 1990); (ii) non-bonded interactions among atoms of the same graphene sheet may be ignored due to the fact that non-bonded terms are weaker than the bonded ones by orders of magnitude; this can be easily proved by comparing the respective terms as calculated by the introduced formulation. Subsequently, the special finite element U99 can be used for modelling the atomic interactions between adjacent graphene sheets. Following the notation of Figure 4, each atom of layer L1 interacts with all atoms of layer L2 within its effective range. The effective range is visualised using the depicted cone; every atom on layer L1 is assigned a similar cone.

In general, the size of the effective range must be appropriately selected balancing computational efficiency and numerical accuracy. However, in practical problems, the effective range is determined primarily by the employed molecular potential equation and the loading conditions. For instance, if the potential function diminishes after e.g. 0.5 nm, it is rather meaningless to define an effective range of 100 nm. Moreover, the selection of the effective range is also effected by the expected atomic displacements – which depend on the loading conditions. If large displacements are expected, then a wider effective range is more suitable; atoms coming in and out of the effective area may cause numerical convergence issues, thus a wider effective range may be used to minimise such effects.

Considering the case presented in this paper (Figure 11), the effective range has been chosen to include all atoms in the opposite layer for the following reasons: (i) the atomic structure is relatively small and the computational load for U99 is very little; (ii) all possible interactions are included, so that more realistic results are obtained; (iii) atoms being too far away are automatically neglected, since the Lennard–Jones diminishes after 0.34 nm; (iv) in the case of "neglected" atoms, the only computational cost induced by the U99 element is the calculation of interatomic distances, which is practically negligible compared to the computational power required by the other finite elements. Clearly, this implements the
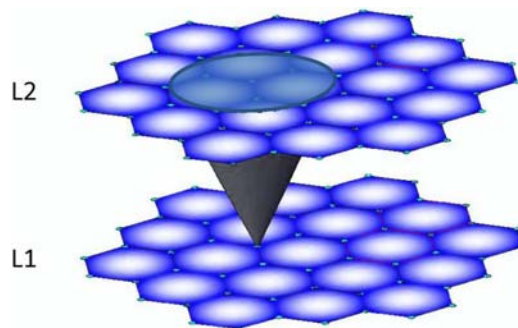
Figure 4.   An assembly of two graphene layers, namely L1 and L2. The effective range of interactions for every atom on L1 is visualised by a cone. The identified atom on L1 should interact with atoms included in the cone base on L2.

computationally worst case scenario, but in this way the upper limit of the required computational may be estimated.

This approach has also the advantage that the atomic pairs to be included in calculations are automatically identified during the analysis; the set of included atomic pairs is appropriately modified and updated based on lattice deformation and relative atomic motion.

Graphene assembly

It has to be clarified that the developed elements cannot, and should not, act independently or unrealistic results will be obtained. For instance, in Figure 2, if the atomic triplet is modelled using only a U3 element and atom "2" moves along the 1–2 direction leaving θ unchanged, this motion will be totally ignored, because U3 "senses" only variations of θ. Therefore, as also implied by the formulation introduced earlier, each graphene layer has to be modelled as an assembly of overlapping U2, U3 and U4 finite elements, while interlayer interactions are represented by U99 elements.

Regarding the implementation of this "element overlap", various techniques may be employed, including coupled nodal motion, etc. Such methods induce, however, additional computational cost and raise questions about the application of loads. In this work, the "over-
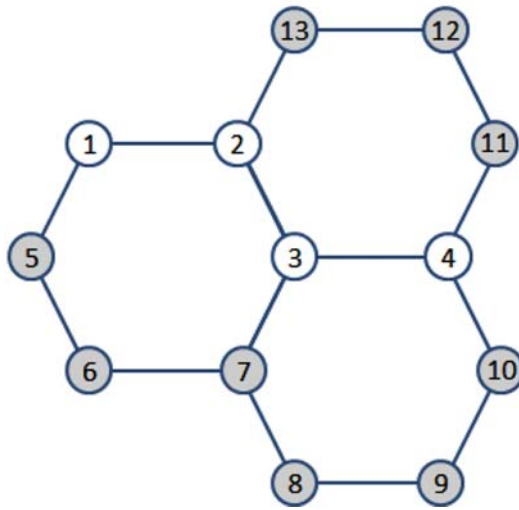
Figure 5. Graphene system with numbered atoms for defining the developed finite elements enlisted in Table 2.

Table 2. List of finite elements required for the representation of the interactions among atoms 1–2–3–4 in Figure 5.

ID	Interaction type	FE type	Involved atoms/nodes
1	Bond stretching	U2	1,2
2	Bond stretching	U2	2,3
3	Bond stretching	U2	3,4
4	Angle bending	U3	2,1,3
5	Angle bending	U3	3,2,4
6	Dihedral angle	U4	1,2,3,4

lapping elements" have been implemented by defining finite elements sharing common nodes. Using this approach, additional computational cost is avoided, since no additional degrees of freedom are included nor any restraining equations are required.

An example is demonstrated in Figure 5. A small group of atoms is depicted, in order to keep the figure simple and clear. As already mentioned, carbon atoms coincide with the nodes of the FE model. Numbering has been used in order to uniquely identify each atom. For this example, only the atoms 1–4 will be considered, therefore, all others have been marked in grey. The following interactions may be identified among these atoms: (i) bond stretching between atoms 1 and 2; (ii) bond stretching between atoms 2 and 3; (iii) bond stretching between atoms 3 and 4; (iv) angle bending for the angle formed by bonds 2–1 and 2–3; (v) angle bending for the angle formed by bonds 3–2 and 3–4; and (vi) dihedral angle interaction affecting atoms 1–2–3–4. These interactions can be expressed in the FE formulation by defining finite elements enlisted in Table 2. All atomic interactions in a graphene sheet may be represented in the same way.

Incorporation into FE codes

The introduced formulation has been developed targeting incorporation into well-established FE codes. As an example, incorporation into Abaqus® (Dassault Systemes) will be discussed. Four different user-defined finite elements have been developed using the subroutine UEL, each one expressing an individual type of interaction in Equation (1). For simplicity reasons, they are termed as U2, U3, U4 and U99, respectively, following the nomenclature used for the developed finite elements earlier.

The definition of each element requires: (i) the calculation of internal forces and (ii) the calculation of the element stiffness matrix:

$$f_i = -\frac{\partial V}{\partial u_i}, \quad A_{ij} = \frac{\partial^2 V}{\partial u_i \partial u_j}, \tag{58}$$

where f_i is the force component due to the ith degree of freedom and A_{ij} is the contribution of the ith and jth degrees of freedom to the global stiffness, following the notation of Abaqus. The assembly of the global matrices and application of external loads is performed automatically by the FE Solver.

Abaqus has no means to identify the geometrical details of a user defined element and its visualisation capabilities are limited to plotting nodes. Thus, an alternative visualisation method has to be pursued. Using simple truss element overlapping, every U2 element provides a very simple way to visualise atomic bonds (Figure 6(a)). If multiple graphene layers are modelled, the "truss visualisation" becomes confusing, and membrane elements are used to fill the hexagonal lattice (Figure 6(b)). In both cases, the material assigned to the "visualisation elements" has practically no stiffness ($E = 1\mathrm{e}{-}30\,\mathrm{Pa}$), so that there is no contribution to the response of the structure.

Regarding the solver, the general static solver of Abaqus® is used for the simple demonstration cases that follow. Loads are incrementally applied. Although the load increment has no impact on the final results, it affects the convergence of the solution. A large load increment will lead to large atomic displacements; in this case, various energy terms are eliminated and cause the stiffness matrix to become singular and the simulation to be prematurely terminated. On the other hand, the selection of too many small load increments may lead to very long solution times. It has been observed that good convergence is obtained if the
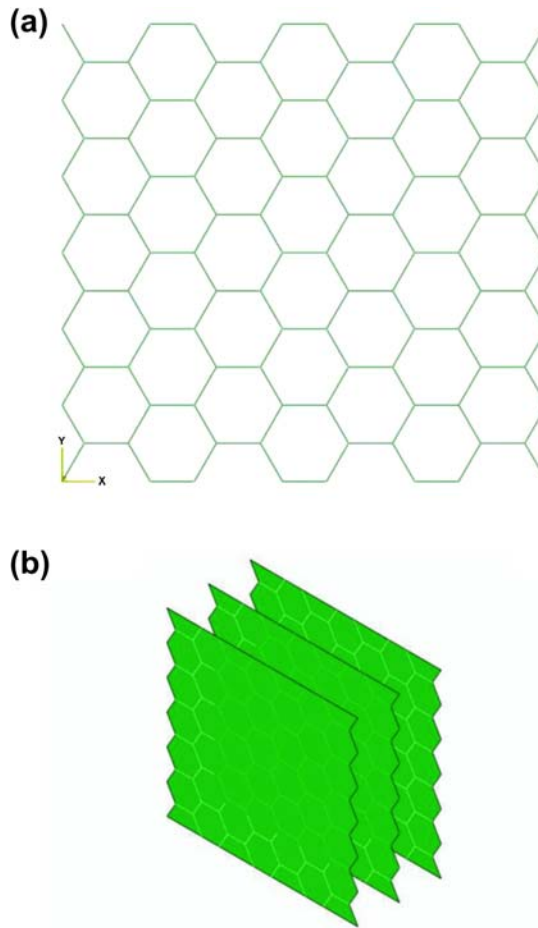
Figure 6.   Visualisation of graphene in Abaqus. (a) A single graphene layer is visualised using truss elements. (b) Complex structures are better visualised using membrane elements.

atomic displacements do not exceed 10% of the undeformed bond length at each load increment. Work in progress focuses on local instabilities and failure under compressive loads using the Riks Solver, but these results have not been validated yet and they are left out of this paper.

Application cases

A series of simple load cases have been examined to evaluate the capabilities of the presented approach. It has to be noted that the employment of analytical equations for molecular mechanics and the avoidance of any approximation or interpolation schemes ensures that the energy calculations for every atomic configuration will be the same as if calculated by a dedicated molecular mechanics code.

The load cases presented in following are applied on relatively small structures for visualisation purposes. The size of the investigated atomic configuration is practically limited only
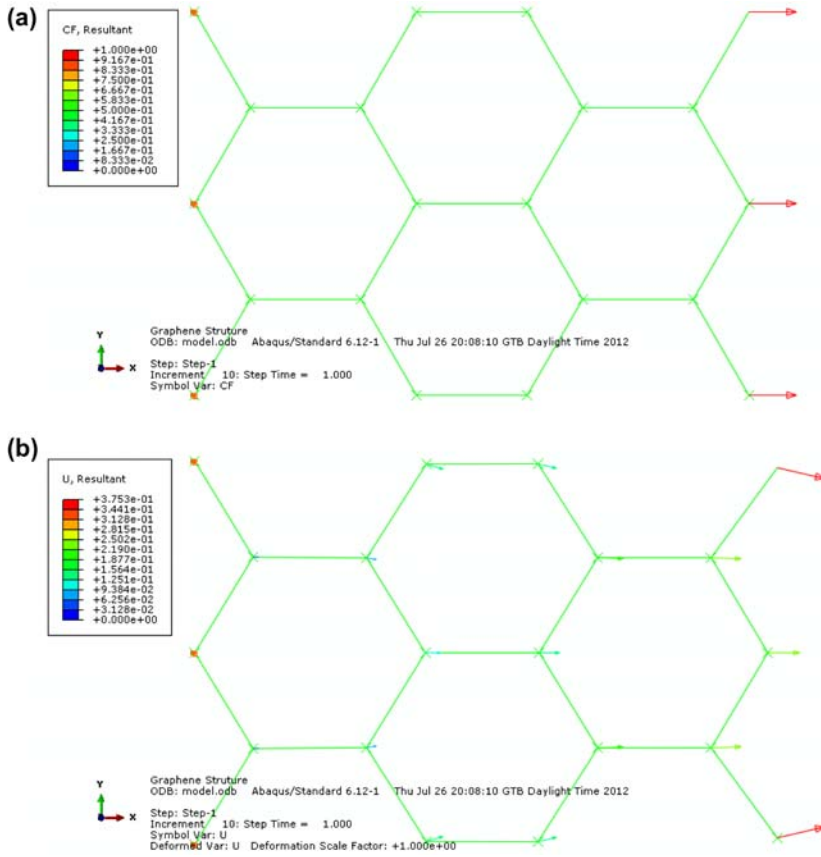
Figure 7. Graphene subjected to tension. (a) Undeformed lattice; arrows show the applied load. (b) Deformed lattice; arrows show the resultant atomic displacements.
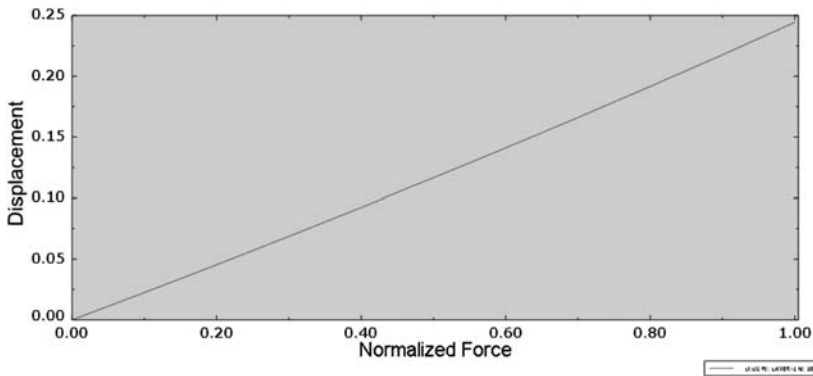
Figure 8. Tip displacement in Angstroms vs. the normalised value of the applied load.

by the availability of computational resources. Graphene modelling with user elements has practically no limitations other than those imposed by the molecular mechanics formulation.
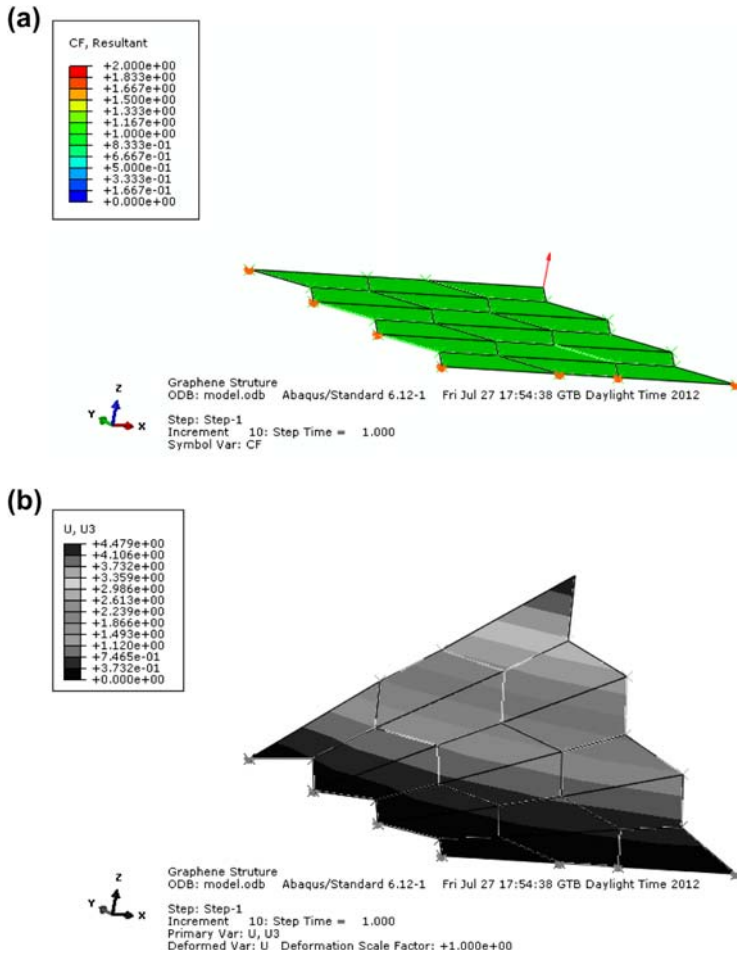
Figure 9.   Graphene subjected to out-of-plane loading. (a) Initial configuration. (b) Deformed shape.
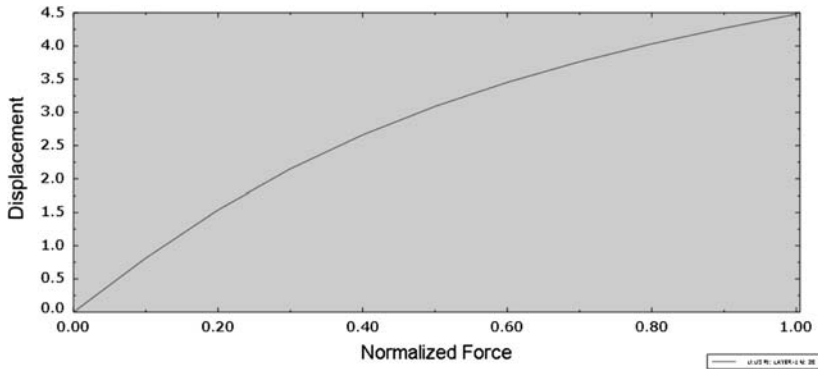
Figure 10.   Out-of-plane displacement of the loaded atom vs. the normalised value of the applied load. Displacement is expressed in Angströms.
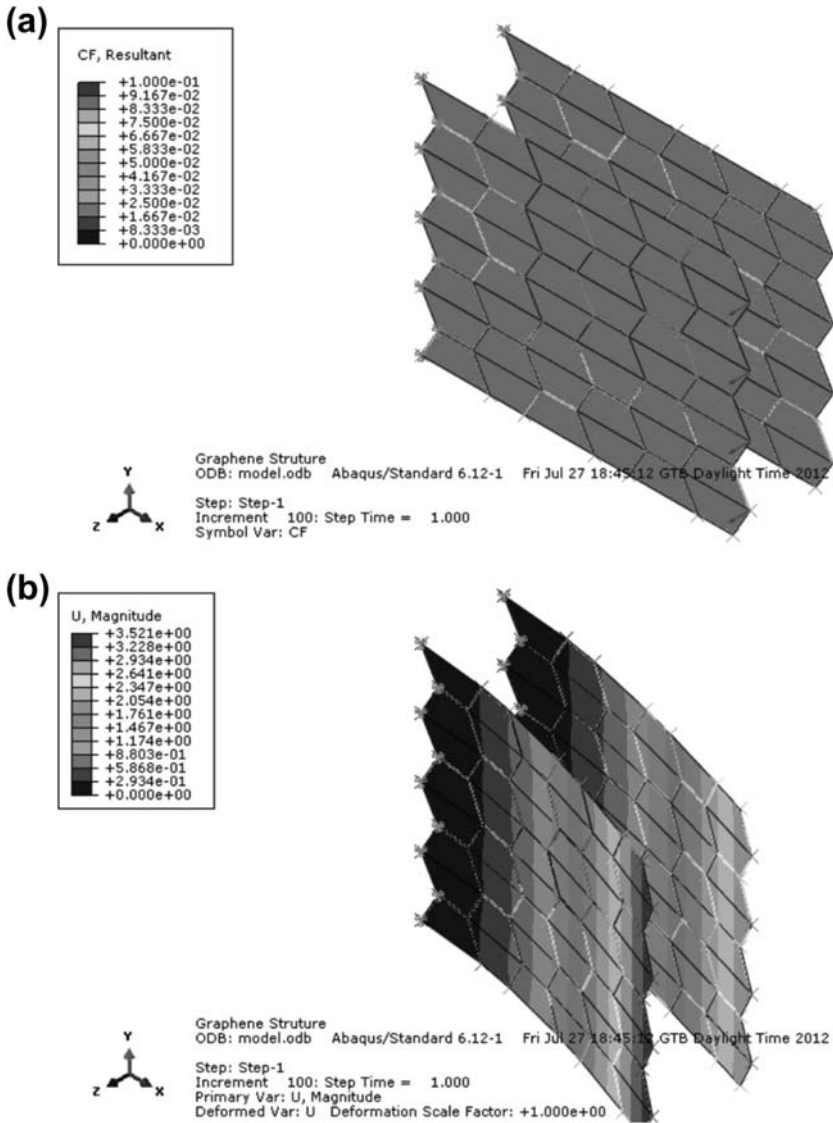
Figure 11.   Bilayer structure. (a) Initial configuration. (b) Deformed shape.

This means that graphene models in Abaqus will continue to run even if the valid range of the molecular equations is exceeded, resulting, of course, to non-realistic atomic configurations. It is, therefore, the analyst's responsibility to interpret results; future work will focus on the inclusion of bond breaks and nanoscale failure issues.

For each load case presented in the following, it is implied that loading is applied on a relaxed atomic structure. When dealing with structures like graphene, where – ideally – atomic distances and angles are well known, it is feasible to define an initial configuration very close to the relaxed state of the system. If this initial configuration is left unloaded, the proposed modelling approach will eventually bring it to a relaxed state. After the relaxed state has been obtained, load may be applied.
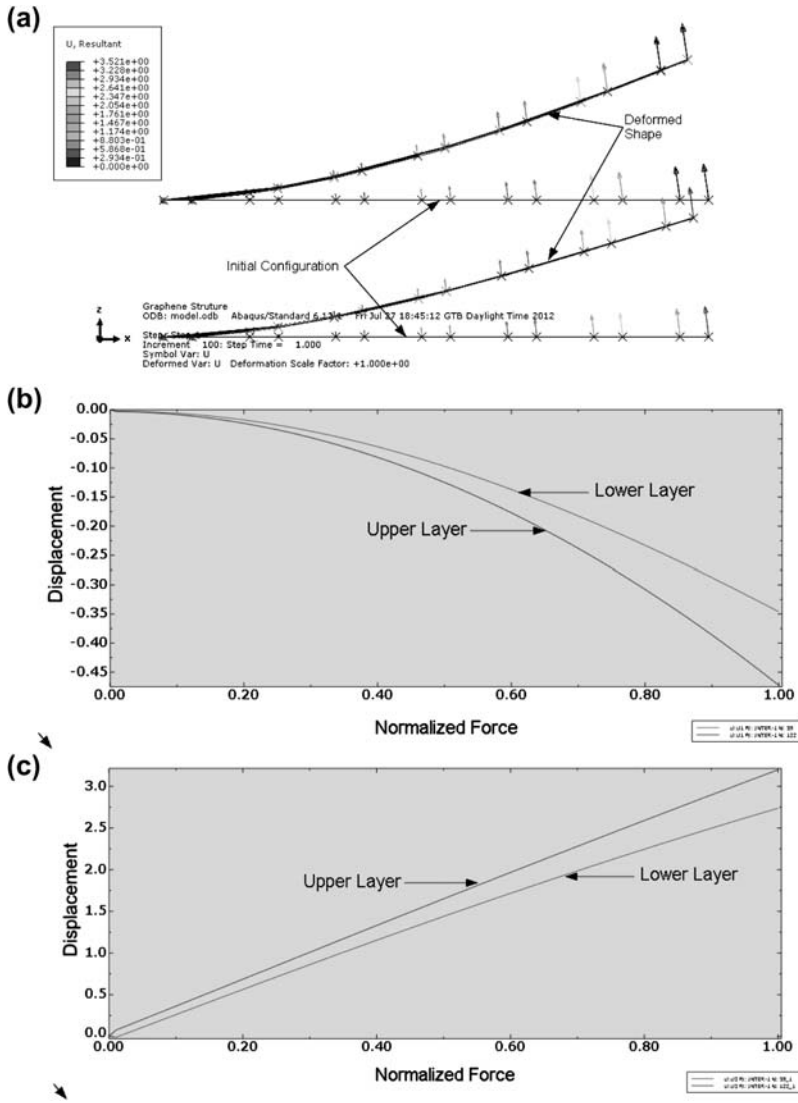
Figure 12. Atomic displacements. (a) The length of the arrows is correlated to the displacement magnitude. (b) Displacement at the layer tip along *x*-direction. (c) Displacement at the layer tip along *z*-direction. All displacements are expressed in Angströms.

In all cases, load appears as a normalised value, i.e. the ratio of the force magnitude in each load step over the magnitude of the maximum force applied.

Case 1: tension

The graphene part depicted in Figure 7(a) is subjected to tension. The three left side atoms are fixed in place. A horizontal force of magnitude 1.6022 nN (i.e. 1 eV/Å) is applied on each of the three right side atoms. The structure containing 20 atoms has been modelled using 23 U2,

36 U3 and 54 U4 elements. Load is applied incrementally and results are depicted in Figure 7 (b). The arrows on nodal positions denote the magnitude of atomic displacements. Figure 8(a) shows the axial displacement on the right edge of the structure vs. the normalised value of the applied load; linear response is exhibited, while Poisson's effect is obvious (Figure 7(b)).

Case 2: out-of-plane loading

The system depicted in Figure 9(a) is subjected to a more complex load. The atoms on the right and bottom edges are fixed in place, while an out-of-plane concentrated force is applied on the upper right atom. Results are shown in Figures 9(b) and 10 where the deformed shape and the out-of-plane displacement of the loaded atom vs. the applied load, respectively, are depicted.

Case 3: graphene bilayer

Two graphene layers separated by 0.34 nm, i.e. the interlayer distance of graphite, are modelled (Figure 11(a)). The atoms of both layers are fixed in place along the left side of the structure. Load is applied on the atoms of the front layer along the right side; force has components along the positive z-axis and the negative x-axis. Although this is a very simple model for demonstration purposes only, this "pealing process" resembles the exfoliation of graphite for the production of graphene. The deformed shape is shown in Figure 11(b). The major difference compared to the previous cases is the existence of non-bonded interaction finite elements (U99) to model the interlayer interactions. The displacement of atoms is monitored (Figure 12). Initially, the bottom layer follows the motion of the upper one due to the van der Waals forces developed between the two layers. As the displacement of the upper atoms increases, the interlayer forces become weaker and due to the dominant in-plane interactions the lower layer seems to have increased flexural stiffness. The snapshot depicted in Figures 11 and 12 is the final stable configuration under the loading condition applied; after
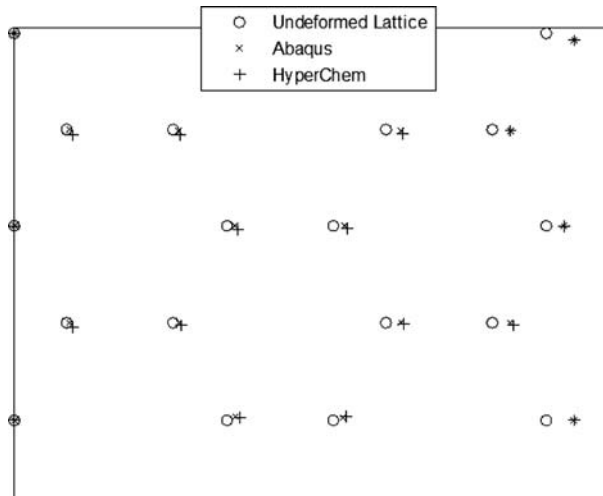
Figure 13.   Results validation for the case of tensile loading. Circles denote the atomic positions at the Initial Configuration (undeformed lattice). The predictions of Abaqus and HyperChem are practically the same, within a reasonable range of numerical accuracy. The atomic bonds are left out of this plot for clarity reasons.
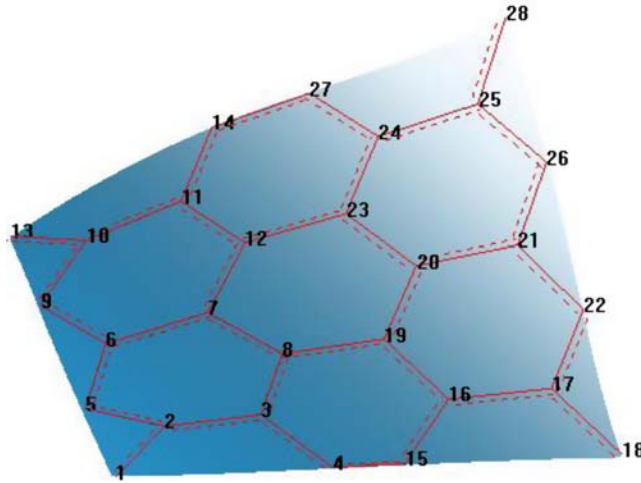
Figure 14. Deformed shape for out-of-plane loading; the response predicted by HyperChem follows the one depicted in Figure 9 (Abaqus prediction).

that local instabilities and nanobuckling initiate, but further investigation for validity is required before results are presented.

Validations

Results have been validated using HyperChem 7.5. The same atomistic system has been modelled once using the introduced approach, and once using HyperChem and the MM + molecular mechanics potential. Figure 13 demonstrates comparisons for Case 1 (Tension). Atomic positions for each atomic configuration are plotted on the same coordinate system. Circles denote the atomic positions in the Initial Configuration – termed as undeformed lattice. After loads have been applied, atoms move to their new equilibrium positions. These are depicted using " × " for Abaqus predictions and " + " for HyperChem predictions. For clarity reasons, atomic bonds have been left out of this plot. Results are almost identical, within the range of reasonable numerical accuracy.

The same behaviour can be observed for the other cases as well, but due to the 3D geometry involved, the corresponding figures are difficult to read and rather confusing. Therefore, the corresponding equilibrium state for out-of-plane loading is depicted separately in Figure 14 in order to demonstrate that the same trend is observed.

Summary

Graphene has been modelled using specialty finite elements based on analytical expressions of molecular mechanics. The goals of the proposed approach are: (i) to be user-friendly for users without long experience in molecular modelling; the creation of an atomistic model is practically the same as the modelling of truss structure, with the addition, of course, of the overlapping user-elements and (ii) to provide some capabilities not available in many dedicated molecular mechanics software packages, like the application of concentrated loads on individual atoms. The introduced method can analyse systems of any size, limited only by the available computational equipment and resources. As an example, the developed finite

elements have been incorporated into Abaqus and various load cases have been demonstrated. Results have been validated using HyperChem 7.5. Future work will focus on bond breaking and crack propagation.

Acknowledgement

References

Avila, A. F., Eduardo, A. C., & Neto, A. S. (2011). Vibrational analysis of graphene based nanostructures. *Computers & Structures, 89*, 878–892.

Brenner, D. W. (1990). Empirical potential for hydrocarbons for use in simulating the chemical vapor decomposition of diamond films. *Phys. Rev. B, 42*, 9458–9471.

Brownson, D. A. C., Kampouris, D. K., & Banks, C. E. (2011). An overview of graphene in energy production and storage applications. *Journal of Power Sources, 196*, 48733–44885.

Caillerie, D., Mourad, A., & Raoult, A. (2006). Discrete homogenization in graphene sheet modeling. *Journal of Elasticity, 84*, 33–68.

Dassault Systemes. Abaqus Unified FEA. Retrieved from http://www.3ds.com/products/simulia/portfolio/abaqus/overview/

Gaim, A. K., & Novoselov, K. S. (2007). The rise of graphene. *Nature Materials, 6*, 183–191.

Geim, A. K. (2009). Graphene: Status and prospects. *Science, 324*, 1530–1534.

Jones, J. E. (1924). On the determination of molecular fields-II: From the equations of state of gas. *Proceedings of the Royal Society of London, 106*, 463–477.

Le Dret, H., & Raoult, A. (2011). Homogenization of hexagonal lattices. *Comptees Rendus Mathematique, 349*, 111–114.

Natsuki, T., & Endo, M. (2004). Stress simulation of carbon nanotubes in tension and compression. *Carbon, 42*(11), 2147–2151.

Parvaneh, V., Shariati, M., Torabi, H., & Sabeti, A. M. M. (2012). Torsional buckling behaviour of SWCNTs using a molecular structural mechanics approach considering vacancy defects. *Fullerenes, Nanotubes and Carbon Nanostructures, 20*, 709–720.

Poetscke, M., Rocha, C. G., Foa Torres, L. E. F., Roche, S., & Cuniberti, G. (2010). Modeling graphene-based nanoelectromechanical devices. *Physical Review B, 81*, 193404.1–193404.4.

Sakhaee-Pour, A., Ahmadian, M. T., & Naghdabadi, R. (2008). Vibrational analysis of single-layered graphene sheets. *Nanotechnology, 19*(085702), 1–7.

Shi, Z., Lu, H., Zhang, L., Yang, R., Wang, Y., Liu, D., … Zhang, G. (2012). Studies of graphene-based nanoelectromechanical switches. *Nano Research, 5*, 82–87.

Suli, E., & Mayers, D. F. (2003). *An introduction to numerical analysis*. New York, NY: Cambridge University Press.

Sun, Y., Wu, Q., & Shi, G. (2011). Graphene based new energy materials. *Energy & Environmental Science, 4*, 1113–1132.

Theodosiou, T. C., & Saravanos, D. A. (2007). Molecular mechanics based finite element for carbon nanotube modeling. *Computer Modeling in Engineering & Science, 19*, 121–134.

Tserpes, K. I. (2012). Strength of graphenes containing randomly dispersed vacancies. *Acta Mechanica, 223*, 669–678.

Ypma, T. J. (1995). Historical development of the Newton–Raphson method. *SIAM Review, 37*, 531–535.